electronics

MDPI

Article

A Repetitive Low Impedance High Power Microwave Driver

Hanwu Yang *, **Zicheng Zhang**, **Jingming Gao**, **Tao Xun** and **Song Li**

College of Advanced Interdisciplinary Studies, National University of Defense Technology,
Changsha 410073, China; zczhang@nudt.edu.cn (Z.Z.); jingming@nudt.edu.cn (J.G.); xuntao@nudt.edu.cn (T.X.);
lisong111@nudt.edu.cn (S.L.)
* Correspondence: yanghw@nudt.edu.cn

Abstract: A low impedance high power microwave (HPM) driver is designed, which can be used in studying multi-gigawatt HPM devices such as the magnetically insulated transmission line oscillator (MILO), based on a helical pulse forming line (PFL) and the Tesla pulse transformer technology. The co-axial PFL is insulated by ethanol–water mixture, whose dielectric constant can be adjusted; and the helical line increases the output pulse width as well as the impedance to make a better match with the load. By the optimal combination of PFL charging voltage and output switch working voltage, the reliability of the PFL can be improved. The Tesla transformer has partial magnetic cores to increase the coupling coefficient and is connected like an autotransformer to increase the voltage step-up ratio. The primary capacitor of the transformer is charged by a high voltage constant current power supply and discharged by a triggered switch. A transmission line is installed between the PFL and the HPM load, to further increase the load voltage. A ceramic disk vacuum interface is used for improving the vacuum of the HPM tube. The experiments show that the driver can operate at 30 GW peak power, 75 ns pulse width and 5 Hz repetition rate.

Keywords: pulsed power; pulse forming line; Tesla transformer; repetitive operation; high power microwaves

check for updates

Citation: Yang, H.; Zhang, Z.; Gao, J.; Xun, T.; Li, S. A Repetitive Low Impedance High Power Microwave Driver. *Electronics* **2022**, *11*, 784. https://doi.org/10.3390/electronics11050784

Academic Editor: M. Tariq Iqbal

Received: 4 January 2022
Accepted: 1 March 2022
Published: 3 March 2022

1. Introduction

Pulsed power technologies have many applications in both industrial and military fields [1,2], and pulse generators come in various sizes and parameters, with the 33 m diameter, 80 TW Z machine in Sandia [3] and a laptop sized 50 kV, 10 kV/ns rising rate trigger generator [4]. High power microwave (HPM) is one of the important applications of pulsed power and it has gained rapid development in recent years due to its potential use in directed energy weapons, power beaming, plasma heating and cancer treatment [5,6], etc. Since HPM studies require a special category of compact, repetitive pulse generators (electron beam accelerators), pulsed power drivers especially devoted to HPM are also widely researched, and they also have a very wide range of parameters in peak power, pulse width, impedance, rep-rate, etc. For example, a promising HPM device, the magnetically insulated transmission line oscillator (MILO) [7–11], which is compact and requires no guiding magnetic field, requires a low impedance HPM driver of the following electrical parameters: power in the range of tens gigawatt, impedance around 10 Ω, pulse width around 100 ns, repetition rate of 1–10 Hz, etc. The accelerators should also be as compact, efficient, and reliable as the state-of-the-art technology can achieve at a reasonable cost.

The past decade has seen various custom-built HPM drivers around the world, using very different technical approaches [12–22], with peak power ranging from several to several tens of gigawatts. Most of the drivers have a water or oil filled coaxial or Blumlein pulse forming lines (PFL). For example, the very successful SINUS series accelerators from the Institute of High Current Electronics, Tomsk, Russia, featuring in transformer oil insulated PFLs with built-in Tesla transformers, have been widely used [12,13]. They are suitable for driving high impedance (>50 Ω) HPM tubes such as the BWO [23] since the oil insulated PFL has characteristic impedance in the range of dozens of ohms. For lower impedance (<20 Ω) requirements, water or aqueous based liquid mixture may be used as they have a higher dielectric constant than transformer oil [22,24]. Some other accelerators have no pulse forming lines, as they use a Marx generator or a linear transformer driver (LTD) with a very short rise time [14,15,21] or with a pulse forming network (PFN) [19,20], and the output pulse width is not limited by the geometry length of the driver. These PFL-less drivers are also aimed at driving the high impedance HPM loads and they have much more components than drivers with pulse forming lines.

This paper presents a 30 GW, 75 ns, 5 Hz rep-rate HPM driver with liquid helical pulse forming line for low impedance HPM devices. This driver is unique in that it allows optimal energy storage, impedance matching with the load, longer pulse width and it is relatively compact and robust. Since the driver was put into use in 2015, several novel or high efficiency MILO studies were carried out, with the frequency in the range of 1.48–16 GHz and peak radiated power of 2–6 GW [9,10,22]. Section 2 describes the main designing considerations of the pulse generator and the details of each part, including the reliability model of the pulse forming line, the partial core pulse transformer, etc. Section 3 shows the experiment results and Section 4 contains a summary.

2. Materials and Methods

2.1. Overview of the HPM Driver

The design of the HPM driver utilized the proven technologies and a modular building method, where each part can be easily assembled, maintained, improved, or replaced if it fails or a better alternative technology is available. The block diagram of the driver is shown in Figure 1. The primary capacitor is charged by a high voltage direct current (HVDC) power supply and discharged by a triggered primary switch. The energy in the capacitor is transferred to a liquid helical PFL via a step-up Tesla transformer. The output switch is a self-break gas switch and when voltage achieves preset level, the energy in the PFL is transferred to a vacuum diode load such as a MILO via a transmission line (TL). The TL serves as an impedance transformer to make MILO's impedance better matched to PFL. The vacuum diode has a ceramic disk insulator so that it has a very low outgassing rate and a high vacuum level could be achieved.

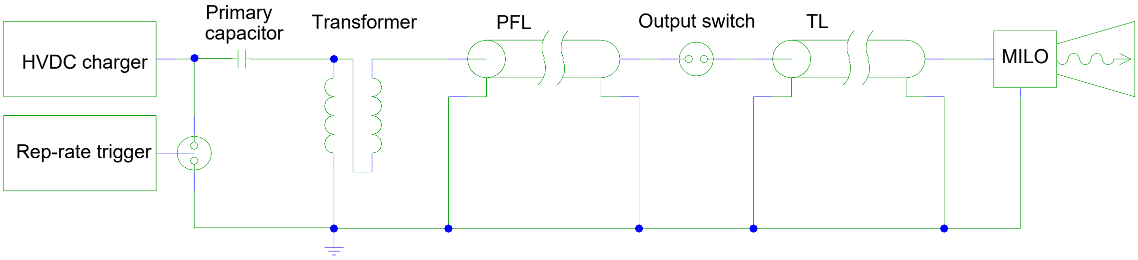

Figure 1. Schematic of the HPM driver.

Figure 2 shows the photo of the developed HPM driver, where the main building blocks, such as the HVDC charger, the primary capacitor, the transformer, the PFL, the output switch, and the transmission line, etc., are marked out. The liquid processing unit for the liquid mixture is outside of the photo. Remote control of the driver is realized by starting the HVDC charger and triggering the primary switch through optical fibers.

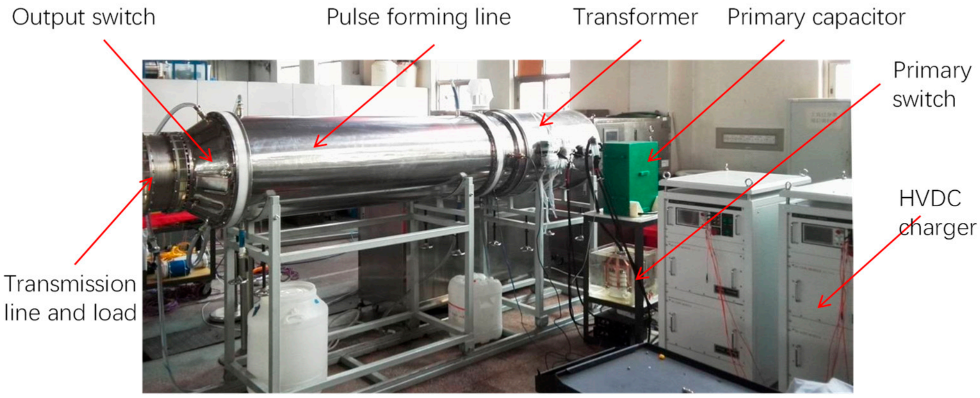

Figure 2. Photo of the HPM driver.

2.2. Design Considerations of the Key Components

2.2.1. Liquids Dielectric Mixtures

Though solid-state pulse generators are becoming popular these days, we prefer the liquid pulse forming line technology for its low cost and the advantages of the liquid material over the solid one simply because of the liquid's fluidity, which makes heat dissipation, fast recovery, good electrode contacts, and high electric strength possible or easy to achieve [24]. We particularly favor the aqueous mixtures, such as glycol, glycerin, and ethanol, as they have high, adjustable dielectric constant, higher resistivity, and a higher range of operation temperature than pure water, and these characteristics offer additional design freedoms, in addition to their high energy storage density to make the PFL compact [22]. Low dielectric constant liquids, such as transformer oil, are not suitable to use for low impedance pulse forming lines, and the line length will be much longer than practical for a pulse width of about 100 ns.

In this study, a 50% volume fraction ethanol–water mixture is used. The mixture has a dielectric constant of about 52 and it has higher resistivity (>50 MΩ·cm) after deionization treatment compared to pure water (~18 MΩ·cm). Even with the deionization device turned off for 24 h, the ethanol–water mixture can maintain its resistivity to above 20 MΩ·cm; hence, it is not necessary to run the deionization device continuously. In addition, the mixture has a lower melting point which allows the PFL to temporarily work outdoors in winter. Figure 3a shows the mixture's density (in unit g/cm^3) and relative dielectric constant vs the volume fraction of ethanol, and Figure 3b shows the measured liquid resistivity decreasing with time after the deionization device is turned off. Because of the linear relation between the dielectric constant and volume fraction of the ethanol, the tailoring of the dielectric constant to a desired value is made easy.

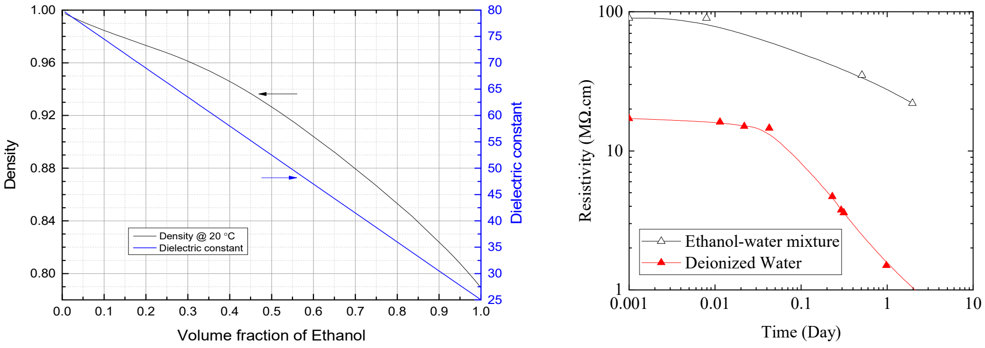

(**a**) (**b**)

Figure 3. (**a**) Relation between the density, relative dielectric constant of ethanol–water mixture, and the volume fraction of ethanol; (**b**) The mixture has a higher resistivity than deionized water and its decay with time is also slower.

2.2.2. Helical Pulse Forming Line

A coaxial transmission line has its characteristic impedance determined by the dielectric constant ε_r and the line's inner and outer radius r_i, r_o, i.e., $Z_0 = \frac{60}{\sqrt{\varepsilon_\mathrm{r}}} \ln \frac{r_\mathrm{o}}{r_\mathrm{i}}$ Ω. The line has a specific impedance to optimize its energy storage, as having very low values of r_i causes field enhancement at the inner conductor's surface and very high values of r_i decreases the gap between the inner and outer conductors. The optimal impedance for energy storage is $30/\sqrt{\varepsilon_\mathrm{r}}$ Ω, which is about 3.3 Ω for deionized water, having a dielectric constant $\varepsilon_\mathrm{r} = 81$. This impedance is much less than the load impedance, which is usually above 10 ohms for MILO; hence, the energy efficiency from PFL to load is poor. By using the ethanol–water mixture, the impedance can be increased at the cost of less output pulse length.

To address such a dilemma of optical impedance and pulse width, a coaxial helical pulse forming line is developed, following the method in reference [25]. References [26–28] give the analysis and simulation of the helical structure. The main idea is that during the slow charging period, the helical inner cylinder works essentially like a straight cylinder, and the inner conductor radius is optimized to have maximum energy storage; during the fast pulse forming period, the helical line is practically a slow wave structure, and as a result, the output pulse width is lengthened, and the apparent impedance is increased. By adjusting the slow wave coefficient, we can make the PFL's output impedance better matched to that of the load. Thus, the helical structure makes the following possible simultaneously: optimized energy storage, optimized impedance matching, and longer output pulse width than a straight forming line. Figure 4 shows the geometry structure of the helical PFL. The inner conductor of Figure 4 has another feature, that there are two parallel helical slots, to make the current path along the inner conductor more uniform and the output waveform more square-like.

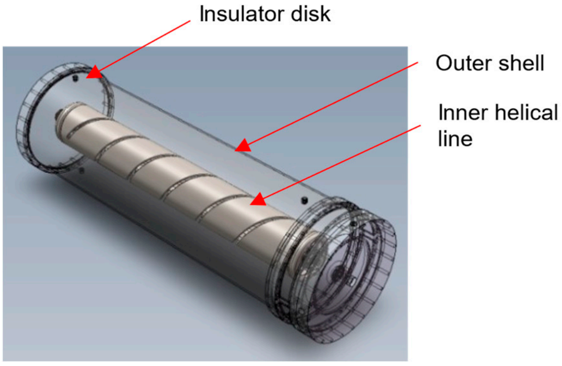

Figure 4. The geometry of the helical forming line.

2.2.3. Reliability Model of the PFL with Output Switch Jitter Considered

One problem of the liquid forming line is that the liquid breaks down randomly, though it can recover its strength after a short period. If the charging time is relatively long, even at a relatively low charging voltage, the breakdown probability is not zero. This problem gets more serious with rep-rate pulsers, as a pulse burst stops prematurely if one pulse has a breakdown.

During experiments, it is found that the random breakdown voltage fluctuation or scattering of the output switch also affects the reliability. In the following context, the voltage scattering σ is defined as the ratio of the standard deviation of the switch breakdown voltage to the average breakdown voltage. The reason is that during the charging process of the PFL, both the liquid and output spark gap switch are stressed in parallel; if the switch is preset to conduct at a lower voltage (e.g., filled with less gas pressure), it will conduct more readily and the chance the liquid will break down is less. Normal operation requires that the switch conducts and the liquid does not break down.

To further optimize the energy storage of the PFL, the charging voltage should not be too high so that water breaks down easily, and not too low so that the PFL's ability is not fully used; therefore, it is ideal to estimate the reliability beforehand. There exists already abundant research for predicting the water breaking down probability, like the famous Martin formula for predicting the water breakdown electric field E_b, as in Equation (1) [29,30],

$$E_b = \frac{E_c}{t_{ef}^{0.33} A^{0.058}} \tag{1}$$

In Equation (1), E_c is a characteristic electric field strength which is 0.23 MV/cm for water in uniform field, t_{ef} is the stress time of the liquid at 63% peak field (in the unit of µs), and A is the area of the electrode (in the unit of cm^2). It is assumed that Equation (1) also applies to the ethanol–water mixture, except a difference in the constant E_c, so that if V_b is breakdown voltage at 50% probability, then the probability of liquid breakdown at normalized PFL charging voltage $v_{ch} = V_{charging}/V_b$ is given by Equation (2),

$$P_{liquid\_break}(v_{ch}) = 1 - \left(\frac{1}{2}\right)^{v_{ch}^{a}} \tag{2}$$

where $a \approx 1/0.058$ is the area related constant [29].

Equation (3) gives the failure probability F as a function of normalized charging voltage v_{ch}, and normalized mean switch voltage v_{sw},

$$F(v_{ch}, v_{sw}) = 1 - P_{gas\_break}\left(1 - P_{liquid\_break}\right) \tag{3}$$

where $v_{sw} = V_{switch}/V_b$ is the ratio between mean switch voltage and the liquid breakdown voltage at 50% probability. The gas switch breakdown probability is assumed to follow the normal distribution with mean voltage being V_{switch} and relative standard deviation being σ. For the self-break spark gap, σ can be as high as 0.05.

Figure 5 shows a calculation result of the above reliability model. Curves 1 to 4 are the failure probabilities with different switch mean voltage and relative scattering. Curve 5 is the probability of liquid breakdown at different normalized charging voltage from Equation (2). It is shown that both higher switched mean voltage and higher relative scattering leads to higher failure probability. For example, for curve 4, if a switch is preset to conduct at a voltage of $0.7V_b$ (by filling gas to a preset pressure), there exists an optimal charging voltage of $\sim 0.75V_b$ to have best reliability, because lower charging voltage leads to higher probability of switch failing to conduct and higher charging voltage leads to higher probability of liquid breaking down. Curve 4 shows that the best predicted reliability is 99.5% as the failure probability is 0.005. Curve 3 has a higher scattering, and the maximum reliability is lower than curve 4. The reason is that at lower charging voltage, though liquid breakdown probability is low, the gas switch's probability to conduct is even lower, resulting in the liquid breaking down first and the PFL failing; whereas at higher charging voltage, the liquid breaks down more easily.

From the above analysis, there is an optimal combination of charging voltage and switch conduction voltage (preset by the gas pressure for a self-break switch), and the lower switch jitter (voltage scattering) permits higher reliability. Figure 6 shows the combination contour regions for a given reliability and switch voltage scattering $\sigma = 0.02$ or 0.05. For example, to achieve 0.98 reliability, the left graph has a very small region (the red area contained in the 0.98 contour line), while the right graph has a much larger region, with less switch voltage scattering. At a given switch's scattering, to obtain higher reliability, the choice of the charging voltage and switch preset voltage combination becomes narrower.

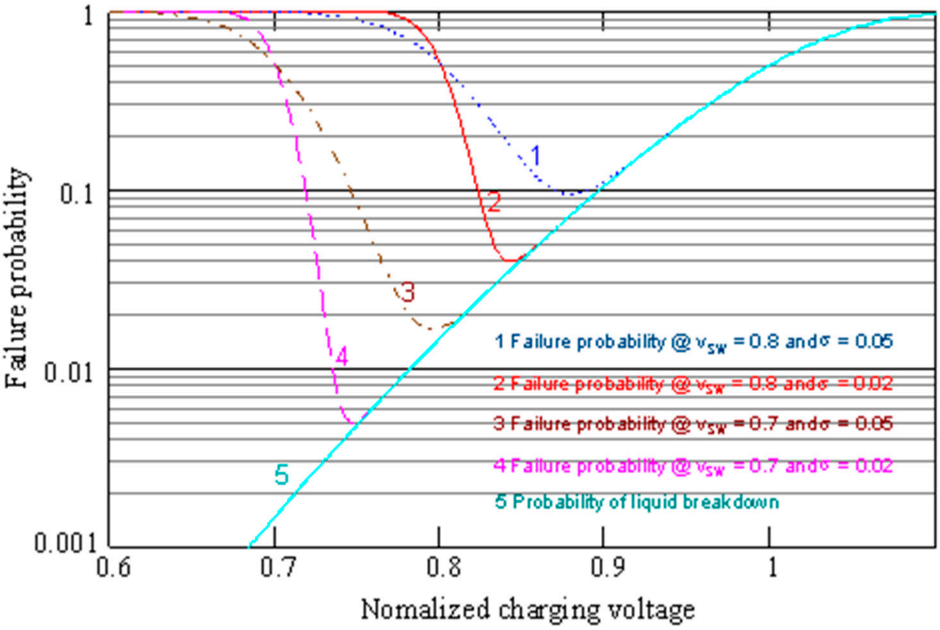

Figure 5. Failure probability of the forming line with switch voltage scattering considered.

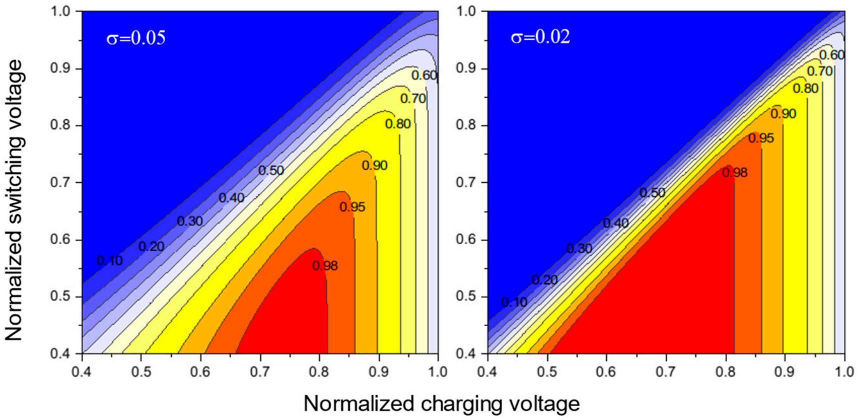

Figure 6. Scattering of switch voltage and combination of charging voltage and switch voltage affect PFL reliability.

2.2.4. Partial Core Pulse Transformer

A Tesla transformer is used to step up the primary voltage and charge the pulse forming line. As the liquid is an aqueous mixture, which has relatively low resistivity (~50 MΩ·cm), a fast charging (<10 μs) is necessary. Fast charging is also required from the liquid breakdown strength relationship, to reduce t_{ef} in Equation (1). Thus, the secondary inductance of the transformer is limited to no more than tens of milli-henries, and the turn ratio is limited to several dozens, and the secondary current is high, so that a transformer with a closed magnetic core is not practical.

An air core transformer was used in a previous single-shot HPM driver [31], which has a relatively low coupling coefficient of about 0.75, so that the energy efficiency from the primary capacitor to secondary PFL is low. Though the coupling coefficient of 0.6 can also achieve ideal efficiency for a Tesla transformer, it is not used here because the PFL voltage will change polarity during the charging period and the liquid breaks down easily under this condition. At last, the partial magnetic core concept [12,32] is adapted and the structure of the transformer is shown in Figure 7a. There are two partial magnetic cores, the inner and the outer core. The primary winding is of 3 turns, installed on the inside surface of the outer core. The secondary winding is about 90 turns, installed on a cardboard skeleton, shown in Figure 7b, to form a cone shape, with the tip of the cone facing the output side. The output of the transformer is connected to the PFL. At the right side of Figure 7 is shown the cardboard skeleton for the secondary winding, immersed in transformer oil. The completed transformer has a coupling coefficient of about 0.95.

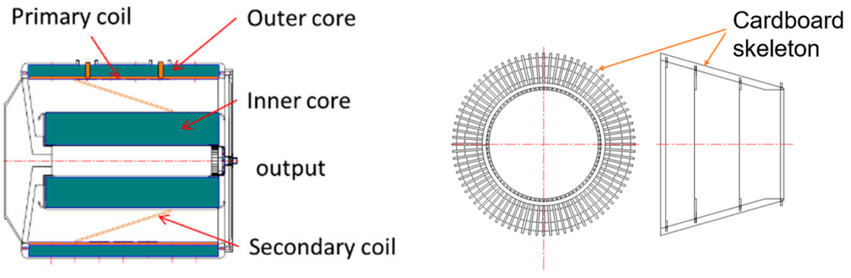

(**a**) (**b**)

Figure 7. Structure of the partial core transformer. (**a**) Cross-section of the Transformer; (**b**) The cone skeleton made of cardboard.

There are two ways to connect the transformer windings, as shown in the top left and bottom left of Figure 8. For the top circuit, both the primary and the secondary winding are connected to the ground. For the bottom circuit, the secondary is not connected to the ground, but to the higher potential side of the primary winding. It is found such an autotransformer connection will increase the output voltage by nearly the primary charging voltage and it is convenient for the geometry in Figure 7, as the higher diameter of the cone winding is connected to the primary's high potential input. The top right and bottom right of Figure 8 give the equivalent circuits of the two transformer circuits, and from these, Equations (4)–(7) can be derived, as the mutual inductance $M = k\sqrt{L_1L_2} = M' = k'\sqrt{L_1'L_2'}$. Equations (6) and (7) give the effective turn-ratio n' and coupling coefficient k' of the autotransformer, and it is easily deduced that the connection in the autotransformer way will increase the turn ratio by almost 1 and the coupling coefficient suffers only a very low decrease, since k is very close to 1, where k and n are the coupling coefficient and turns ratio for the transformer connected in the usual way, as shown in the left circuit of Figure 8.

$$L_1' = L_1 \tag{4}$$

$$L_2' = L_1 + L_2 + 2k\sqrt{L_1L_2} \tag{5}$$

$$n' = \sqrt{\frac{L_2'}{L_1'}} = \sqrt{1 + 2kn + n^2} \approx n + 1 \tag{6}$$

$$k' = \frac{M}{\sqrt{L_1'L_2'}} = \frac{n}{\sqrt{1 + 2kn + n^2}}k \approx k. \tag{7}$$

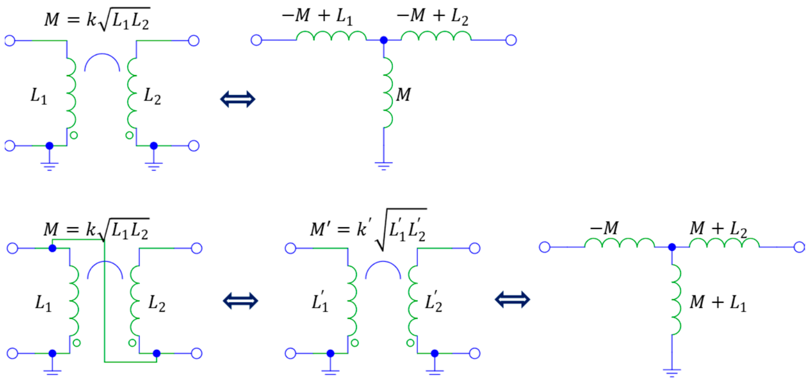

Figure 8. Two connection ways of the transformer circuit and their equivalent parameters.

2.2.5. Other Design Considerations

The high voltage charger for the primary capacitor is composed of four sets of 30 kV, 2 A constant current capacitor chargers [33], with two in parallel and two in series. The charger makes a 5 Hz repetitive operation possible at 50 kV charging voltage. Rep rate can be higher for lower primary charging voltage.

A pseudo spark gap switch (thyratron) of model TDI4-100k/75H [34], as shown in Figure 9a, was used to discharge the primary capacitor. The labeled forward anode voltage of the switch is up to 70 kV, the peak anode current up to 50 kA, and maximum anode current rise rate up to 10^{12} A/s. During the experiments, the switch was connected to the circuit with a coaxial cable, to reduce inductance. The switch performed well initially but degraded quickly after several tens of shots, with frequently pre-firing. Apparently, the dwell time of the peak anode voltage is much longer (~200 ms in our case) than the recommended duration (not higher than 1 ms). Later, a traditional spark gap trigatron switch, shown in Figure 9b, replaced the thyratron. Currently, these switches cannot be turned off when the current goes to zero as thyristors do; hence, energies left in the primary capacitor cannot be reused as is done in SINUS accelerators [12]; but by varying the charging voltage of the primary capacitor, one can make best energy transfer efficiency to the PFL.

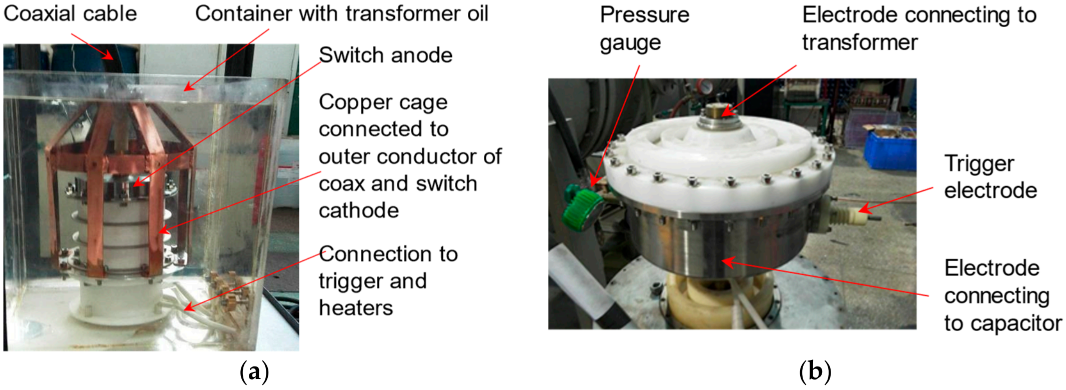

Figure 9. (**a**) Pseudo-spark switch and (**b**) trigatron switch.

The output switch is a spark gap filled with SF_6 at absolute pressure between 0.3–0.4 MPa, and the breakdown voltage is around 1 MV. Special attention is paid to avoid the flashover along the switch envelope's inner surface, which happened occasionally during the initial test. The idea is to decrease the parallel component of the electric field along the envelope surface. Figure 10 shows the potential (contour lines) and the field strength (color shades) of the electrostatic field calculation results of the switch before it breaks down. The electric field in the gap is relatively uniform so that an approximately linear voltage-pressure relationship can be achieved, which makes it easy to adjust switch voltage. On the left side of the figure is the PFL's inner cylinder, whose relatively large radius helps to shield the envelope and the triple point near the switch's left electrode.

A transmission line is installed between the output switch and the load. Though the helical line and the liquid mixture make it easier to match the impedance of the load, it will be more flexible to have another choice. The TL has an impedance value between those of the PFL and the load, serving as a transmission line transformer to make the energy transfer more efficient. In addition, the TL isolates the load from the PFL to mitigate unnecessary voltage reflections.

The vacuum interface of the high-power microwave diode is both a high-voltage feedthrough and a support structure for the cathode. The design of the vacuum interface is very important to its normal operation, and one of the keys is to suppress the occurrence of flashover along the surface [35]. A ceramic liquid–vacuum interface [36–38], as shown in Figure 11, is used to improve the vacuum level within the electron diode and the HPM tube.

The Al_2O_3 ceramic disk is brazed to the outer stainless-steel flange, which has a knife-edge structure so that a metal O-ring can be used to seal the vacuum chamber. This allows high temperature baking of the HPM device to remove absorbed gas, as degassing from organic material or velvet cathode deteriorates the vacuum and limits the rep-rate frequency.

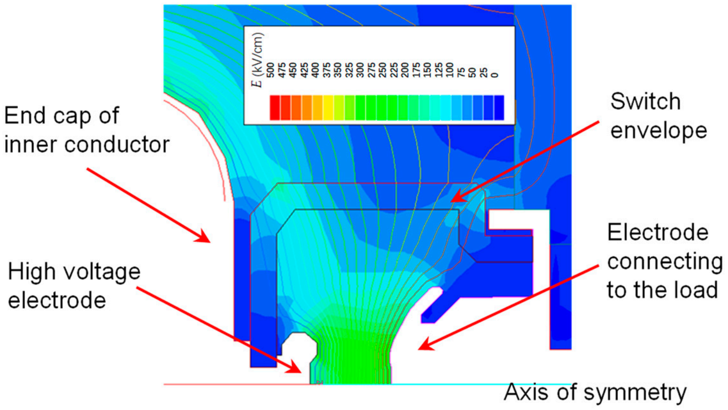

Figure 10. Output switch field distribution.

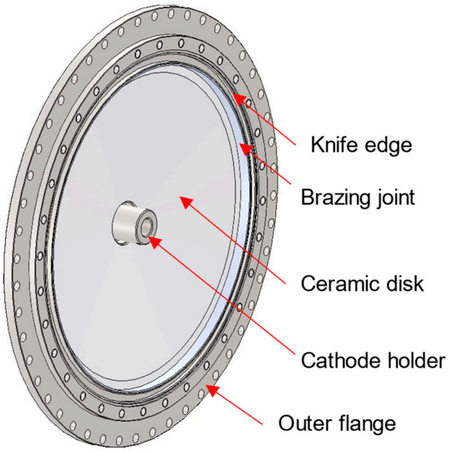

Figure 11. The ceramic liquid–vacuum interface.

3. Results

The circuit parameters of the main components used in the circuit simulation are listed in Table 1. The parameters of the transformer are measured from a LCR meter; the parameters of the PFL and TL are calculated from the geometry of the structures; other equivalent inductance, capacitance, and resistance are estimated values.

Table 1. Circuit parameters used in simulation.

Circuit Parameters	Values	Circuit Parameters	Values
Primary capacitance (C_1)	10 µF	PFL impedance	3.5 Ω
Primary capacitor initial voltage	50 kV	PFL one-way time delay	39 ns
Transformer primary inductance (L_1)	18 µH	TL impedance	7 Ω
Transformer secondary inductance (L_2)	13 mH	TL one-way time delay	40 ns
Transformer coupling coefficient	0.95	Output switch equivalent inductance	130 nH
Equivalent primary serial resistance (R_1)	150 mΩ	Output switch equivalent capacitance	0.1 nF
Equivalent primary inductance (L_1)	110 nH	Equivalent load resistance (R_L)	11 Ω
Equivalent secondary resistance (R_2)	110 Ω	Equivalent load inductance (L_L)	300 nH
Equivalent liquid leaking resistance (R_p)	10 kΩ		

The PSpice circuit schematic is shown in Figure 12a and the simulation results, together with the experimental waveforms, are shown in Figure 12b,c. Qualitatively, the simulation matches the experiment well, and the discrepancy comes from the helical structure which is ignored in the circuit model, and non-ideal response of the measurement probes. Typically, a peak load voltage of 570 kV, current of 52 kA (peak power near 30 GW), and pulsed width (FWHM) 80 ns can be obtained at the load R_L. In theory, peak power can reach 50 GW if the switch is set to conduct later, whereas the PFL must withstand the higher voltage for a longer time and the reliability drops.

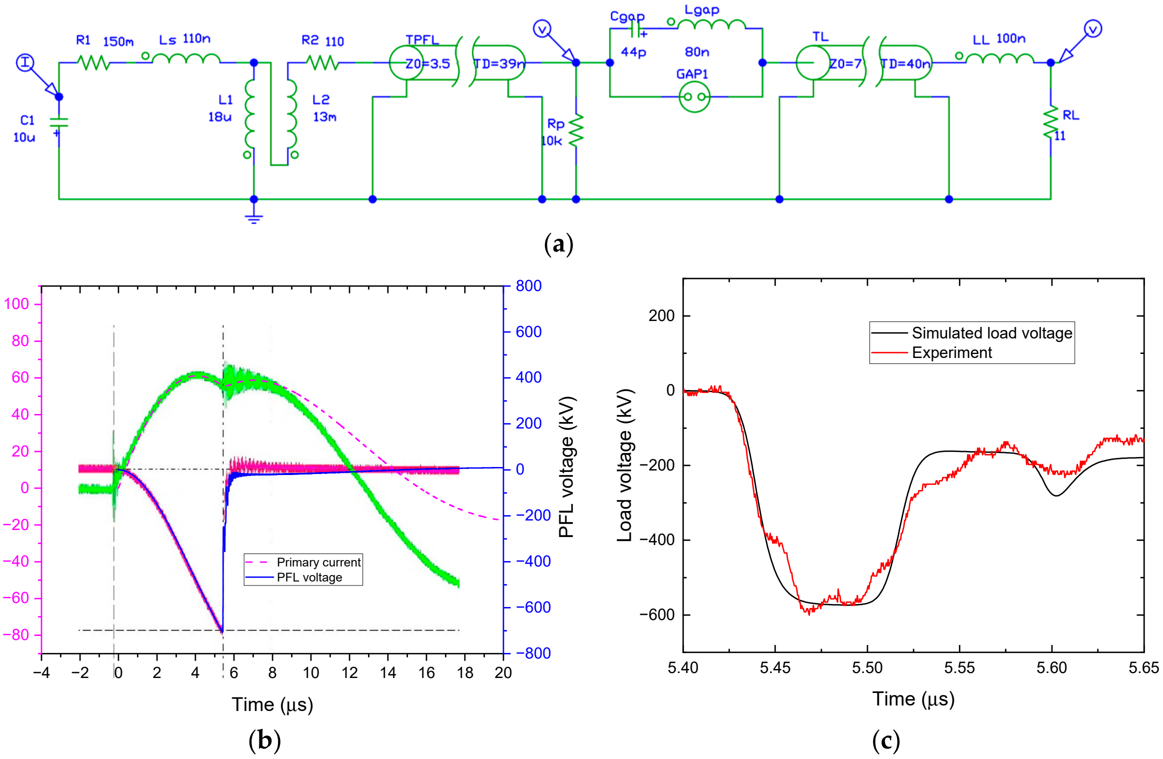

(**a**)

(**b**) (**c**)

Figure 12. Equivalent circuit and simulation results: (**a**) Equivalent circuit; (**b**) Comparison of the primary current and PFL voltage with experiment (green and red curves); (**c**) Comparison of load voltage with experiment (red curve).

The assembled driver is shown in Figure 2, and the maximum diameter of the transformer is 0.6 m, the length of the driver is 4 m, and total weight is about 1.5 ton including the charger. The typical 5 Hz rep-rate waveforms are shown in Figure 13, where the calibrated peak power is above 25 GW, pulse width is 75 ns, and the load is about 11 Ω. The experimental waveforms are like those of the circuit simulation, and the relative switched PFL voltage scattering is less than 3%. During the tests, maximum peak power of 30 GW was achieved, but occasional liquid breakdown (about 1 failure every 30 pulses) caused the train of pulse burst to stop prematurely. From the model in Section 2.2.3, the reliability is estimated to about 0.98. By fine tuning the charging voltage of the primary capacitor at a preset output switch gas pressure (to obtain the desired average output voltage), the reliability can be improved as both too high or too low charging voltage is not desired. In case there is a breakdown event, the experiment can be resumed by turning on the deionization device to filter the liquid and remove the bubbles formed during the breakdown.

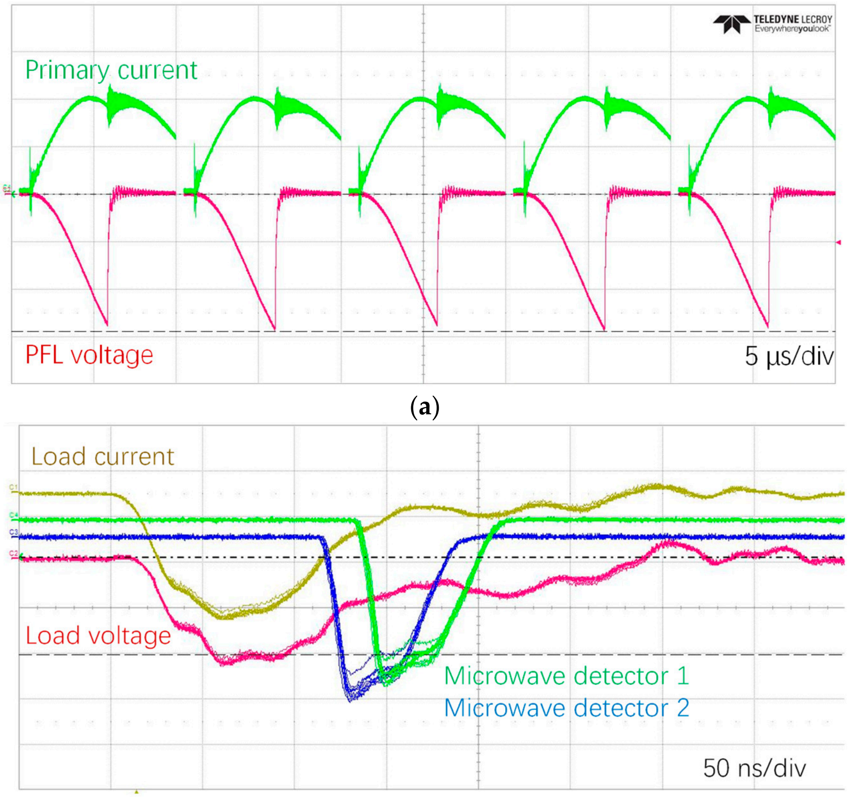

(**b**)

Figure 13. Experiment waveforms of the 5 Hz rep-rate test: (**a**) the primary current of the transformer and PFL voltage; (**b**) the load current, load voltage, and microwave detector signals.

4. Discussion and Conclusions

A rep-rate HPM driver is designed with flexibility and reliability considered. Peak power of 30 GW, pulsed width of 75 ns, rep rate of 5 Hz on a 11 Ω load are obtained. Such a HPM driver is particularly useful for low impedance HPM devices such as MILO. The driver utilizes a modular building method, and each part can be relatively easily assembled, maintained, or updated as better alternative technology is available. The driver is based on a helical pulse forming line (PFL) and the Tesla pulse transformer technology. The co-axial PFL is insulated by water–ethanol mixture, whose dielectric constant can be adjusted; and by adjusting the slow wave coefficient of the helical line, the output pulse width can be increased and better impedance matching with the load can be met. The reliability model of the PFL is analyzed and it is found there is an optimal combination of PFL charging voltage and output switch working voltage. The Tesla transformer has partial magnetic cores to increase the coupling and is connected like an autotransformer to increase the voltage step-up ratio.

In the future, we will continue to optimize the driver, such as: the output switch will be replaced with a triggered one to reduce switch jitter and switch voltage scattering; thus, the reliability will be further improved; the remaining energy in the primary capacitor from previous pulse will be recovered for the next pulse to improve the overall efficiency of the driver.

Author Contributions: Conceptualization, H.Y.; methodology, H.Y., Z.Z., J.G. and T.X.; software, H.Y.; validation, Z.Z., J.G., T.X. and S.L.; formal analysis, H.Y., Z.Z., J.G. and T.X.; investigation, H.Y., Z.Z., J.G., T.X. and S.L.; resources, J.G.; data curation, H.Y.; writing—original draft preparation, H.Y.; writing—review and editing, H.Y.; visualization, H.Y.; supervision, H.Y.; project administration, H.Y.; funding acquisition, H.Y. All authors have read and agreed to the published version of the manuscript.

Funding: This research and the APC were funded by the National Science Foundation of China grant number 51677190 and the leading researcher program of NUDT.

Data Availability Statement: The data that support the findings of this study are available from the corresponding author upon request.

Conflicts of Interest: The authors declare no conflict of interest.

References

1. Mesyats, G.A. *Pulsed Power*; Kluwer Academic/Plenum Publishers: New York, NY, USA, 2005; ISBN 978-0-306-48653-1.
2. Bluhm, H. *Pulsed Power Systems: Principles and Applications*; Springer Science & Business Media: Berlin/Heidelberg, Germany, 2006; ISBN 978-3-540-26137-7.
3. Sinars, D.B.; Sweeney, M.A.; Alexander, C.S.; Ampleford, D.J.; Ao, T.; Apruzese, J.P.; Aragon, C.; Armstrong, D.J.; Austin, K.N.; Awe, T.J.; et al. Review of Pulsed Power-Driven High Energy Density Physics Research on Z at Sandia. *Phys. Plasmas* **2020**, *27*, 070501. [CrossRef]
4. Yan, J.; Parker, S.; Bland, S. An Investigation Into High-Voltage Spiral Generators Utilizing Thyristor Input Switches. *IEEE Trans. Power Electron.* **2021**, *36*, 10005–10019. [CrossRef]
5. Benford, J.; Swegle, J.A.; Schamiloglu, E. *High Power Microwaves*, 3rd ed.; CRC Press: Boca Raton, FL, USA, 2015; ISBN 978-0-429-16064-6.
6. Zhang, J.; Ge, X.; Zhang, J.; He, J.; Fan, Y.; Li, Z.; Jin, Z.; Gao, L.; Ling, J.; Qi, Z. Research Progresses on Cherenkov and Transit-Time High-Power Microwave Sources at NUDT. *Matter Radiat. Extrem.* **2016**, *1*, 163–178. [CrossRef]
7. Fan, Y.-W.; Yuan, C.-W.; Zhong, H.-H.; Shu, T.; Zhang, J.-D.; Yang, J.-H.; Yang, H.-W.; Wang, Y.; Luo, L. Experimental Investigation of an Improved MILO. *IEEE Trans. Plasma Sci.* **2007**, *35*, 1075–1080. [CrossRef]
8. Fan, Y.-W.; Wang, X.-Y.; Zhang, Z.-C.; Xun, T.; Yang, H.-W. A High-Efficiency Repetitively Pulsed Magnetically Insulated Transmission Line Oscillator. *Vacuum* **2016**, *128*, 39–44. [CrossRef]
9. Wang, X.; Fan, Y.; Shu, T.; Li, A.; Yu, Y.; Liu, Z. A High-Efficiency Magnetically Insulated Transmission Line Oscillator with Ridged Disk-Loaded Vanes. *IEEE Trans. Plasma Sci.* **2019**, *47*, 3974–3977. [CrossRef]
10. Wang, X.; Fan, Y.; Shu, T.; Yang, B.; Xu, X.; Li, A.; Liu, Z.; Xu, H. Experimental Demonstration of a Ridged Magnetically Insulated Transmission Line Oscillator. *IEEE Trans. Microw. Theory Tech.* **2021**, *69*, 1698–1702. [CrossRef]
11. Xun, T.; Fan, Y.; Yang, H.; Zhang, Z.; Chen, D.; Zhang, J. A Vacuum-Sealed, Gigawatt-Class, Repetitively Pulsed High-Power Microwave Source. *J. Appl. Phys.* **2017**, *121*, 234502. [CrossRef]
12. Mesyats, G.A.; Korovin, S.D.; Gunin, A.V.; Gubanov, V.P.; Stepchenko, A.S.; Grishin, D.M.; Landl, V.F.; Alekseenko, P.I. Repetitively Pulsed High-Current Accelerators with Transformer Charging of Forming Lines. *Laser Part. Beams* **2003**, *21*, 197–209. [CrossRef]
13. Rostov, V.V.; Stepchenko, A.S.; Vykhodtsev, P.V.; Tsygankov, R.V. High-Voltage Drivers Based on Forming Lines with Extended Quasi-Rectangular Pulses for High-Power Microwave Oscillators. *Electronics* **2022**, *11*, 406. [CrossRef]
14. Rainwater, K.; Barnett, D.; Lynn, C.; Dickens, J.; Neuber, A.; Mankowski, J. A 160 J, 100 Hz Rep Rate, Compact Marx Generator for Driving and HPM Source. In Proceedings of the 2016 IEEE International Power Modulator and High Voltage Conference (IPMHVC), San Francisco, CA, USA, 6–9 July 2016; pp. 228–230.
15. Collier, L.; Walls, M.B.; Dickens, J.; Mankowski, J.; Neuber, A. Solid State Linear Transformer Driver (LTD) Development for HPM Sources. In Proceedings of the 2015 IEEE Pulsed Power Conference (PPC), Austin, TX, USA, 31 May–4 June 2015; pp. 1–4.
16. Novac, B.M.; Istenic, M.; Luo, J.; Smith, I.R.; Brown, J.; Hubbard, M.; Appelgren, P.; Elfsberg, M.; Hurtig, T.; Moller, C.; et al. A 10-GW Pulsed Power Supply for HPM Sources. *IEEE Trans. Plasma Sci.* **2006**, *34*, 1814–1821. [CrossRef]
17. Novac, B.M.; Wang, M.; Smith, I.R.; Senior, P. A 10 GW Tesla-Driven Blumlein Pulsed Power Generator. *IEEE Trans. Plasma Sci.* **2014**, *42*, 2876–2885. [CrossRef]
18. Sporer, B.J.; Shah, A.P.; Dowhan, G.V.; Shapovalov, R.V.; Packard, D.A.; Wisher, M.; Leckbee, J.J.; Hendricks, K.J.; Hoff, B.W.; Lau, Y.Y.; et al. Multicavity Linear Transformer Driver Facility for Z-Pinch and High-Power Microwave Research. *Phys. Rev. Accel. Beams* **2021**, *24*, 100402. [CrossRef]
19. Song, F.; Li, F.; Zhang, B.; Zhu, M.; Li, C.; Wang, G.; Gong, H.; Gan, Y.; Jin, X. Recent Advances in Compact Repetitive High-Power Marx Generators. *Laser Part. Beams* **2019**, *37*, 110–121. [CrossRef]
20. Su, J.; Zhang, X.; Li, R.; Zhao, L.; Sun, X.; Wang, L.; Zeng, B.; Cheng, J.; Wang, Y.; Peng, J.; et al. An 8-GW Long-Pulse Generator Based on Tesla Transformer and Pulse Forming Network. *Rev. Sci. Instrum.* **2014**, *85*, 063303. [CrossRef] [PubMed]
21. Buntin, T.; Abide, M.; Barnett, D.; Dickens, J.; Neuber, A.; Joshi, R.; Mankowski, J. Compact Marx Generator to Drive a Low-Impedance MILO. In Proceedings of the 2019 IEEE Pulsed Power & Plasma Science (PPPS), Orlando, FL, USA, 23–29 June 2019; pp. 1–3.
22. Yang, J.; Zhang, Z.; Yang, H.; Zhang, J.; Liu, J.; Yin, Y.; Xun, T.; Cheng, X.; Fan, Y.; Jin, Z.; et al. Compact Intense Electron-Beam Accelerators Based on High Energy Density Liquid Pulse Forming Lines. *Matter Radiat. Extrem.* **2018**, *3*, 278–292. [CrossRef]
23. Tot'meninov, E.M.; Klimov, A.I.; Kurkan, I.K.; Polevin, S.D.; Rostov, V.V. Repetitively Pulsed Relativistic BWO with Enhanced Mechanical Frequency Tunability. *IEEE Trans. Plasma Sci.* **2008**, *36*, 2609–2612. [CrossRef]
24. Bolund, B.F.; Berglund, M.; Bernhoff, H. Dielectric Study of Water/Methanol Mixtures for Use in Pulsed-Power Water Capacitors. *J. Appl. Phys.* **2003**, *93*, 2895–2899. [CrossRef]

25. Yang, H.; Xu, J.; Zhang, J.; Zhong, H.; Wang, Y.; Fan, Y.; Zhang, Z.; Yang, J.; Luo, L.; Zhao, Y. Experiments of a 30 GW, 100 Ns Compact e-Beam Accelerator. In Proceedings of the IET European Conference on European Pulsed Power 2009. Incorporating the CERN Klystron Modulator Workshop, Geneva, Switzerland, 21–25 September 2009; p. 35.
26. Sharma, S.K.; Deb, P.; Sharma, A.; Shukla, R.; Prabaharan, T.; Adhikary, B.; Shyam, A. Note: Compact Helical Pulse Forming Line for the Generation of Longer Duration Rectangular Pulse. *Rev. Sci. Instrum.* **2012**, *83*, 066103. [CrossRef]
27. Zhang, Y.; Liu, J.L.; Feng, J.H. Effects of Dispersion on Electromagnetic Parameters of Tape-Helix Blumlein Pulse Forming Line of Accelerator. *Eur. Phys. J. Appl. Phys.* **2012**, *57*, 30904. [CrossRef]
28. Wang, L.; Liu, J. Dispersion Analysis of the Solid Helical Pulse-Forming Line. *Laser Part. Beams* **2015**, *33*, 405–413. [CrossRef]
29. Stygar, W.A.; Wagoner, T.C.; Ives, H.C.; Wallace, Z.R.; Anaya, V.; Corley, J.P.; Cuneo, M.E.; Harjes, H.C.; Lott, J.A.; Mowrer, G.R.; et al. Water-Dielectric-Breakdown Relation for the Design of Large-Area Multimegavolt Pulsed-Power Systems. *Phys. Rev. Spec. Top.-Accel. Beams* **2006**, *9*, 070401. [CrossRef]
30. Elizondo, J.M.; Martin, T.H.; Struve, K.W.; Bennett, L.F. The Z-20 Reliability Calculations. In Proceedings of the 14th IEEE International Pulsed Power Conference (IEEE Cat. No. 03CH37472), Dallas, TX, USA, 15–18 June 2003; Digest of Technical Papers. PPC-2003, pp. 895–898.
31. Yang, H.; Xu, J.; Zhang, J.; Zhong, H. Inter-Layer Voltage Distribution and Insulation Failure of a Spiral Pulse Transformer. In Proceedings of the IET European Conference on European Pulsed Power 2009. Incorporating the CERN Klystron Modulator Workshop, Geneva, Switzerland, 21–25 September 2009; pp. P1–P4.
32. Zhang, Z.; Yang, H.; Yang, J.; Chen, D.; Zhang, J.; Zhong, H.; Liu, C. Compact Megavolt Pulse Transformer with Inner Magnetic Core and Conical Secondary Windings. In Proceedings of the 2015 IEEE Pulsed Power Conference (PPC), Austin, TX, USA, 31 May–4 June 2015; pp. 1–5.
33. Zhang, Z.; Liu, Q.; Li, X.; Wu, Z.; Wang, Q.; Yang, H. High Frequency AC-Link Capacitor Charging Power Supply. *High Power Laser Part. Beams* **2012**, *24*, 719–722. [CrossRef]
34. Bochkov, V.D.; Dyagilev, V.M.; Ushich, V.G.; Frants, O.B.; Korolev, Y.D.; Sheirlyakin, I.A.; Frank, K. Sealed-off Pseudospark Switches for Pulsed Power Applications (Current Status and Prospects). *IEEE Trans. Plasma Sci.* **2001**, *29*, 802–808. [CrossRef]
35. Krasik, Y.E.; Leopold, J.G. Initiation of Vacuum Insulator Surface High-Voltage Flashover with Electrons Produced by Laser Illumination. *Phys. Plasmas* **2015**, *22*, 083109. [CrossRef]
36. Xun, T.; Yang, H.; Zhang, J.; Liu, Z.; Wang, Y.; Zhao, Y. A Ceramic Radial Insulation Structure for a Relativistic Electron Beam Vacuum Diode. *Rev. Sci. Instrum.* **2008**, *79*, 063303. [CrossRef]
37. Xun, T.; Yang, H.-W.; Zhang, J.-D. A High-Vacuum High-Electric-Field Pulsed Power Interface Based on a Ceramic Insulator. *IEEE Trans. Plasma Sci.* **2015**, *43*, 4130–4135. [CrossRef]
38. Xun, T.; Zhao, Y.; Yang, H.; Hu, T.; Zhang, Z.; Cheng, X.-B.; Zhang, J.; Zhang, J.; Zhong, H.-H. Developments of Pulsed Electron Beam Sources for High-Power Microwave Applications. *IEEE Access* **2020**, *8*, 101351–101358. [CrossRef]